Proceeding the Regional Conference on Chemical Engineering 2014
Yogyakarta, December 2-3, 2014

ISBN: 978-602-71398-0-0

Synthesis and characterization of highly ordered solid acid catalyst from kaolin

[1] Peter Adeniyi Alaba, [1,2] Yahaya Muhammad Sani & [1] Wan Mohd Ashri Wan Daud

[1]Department of Chemical Engineering, University of Malaya, 50603 Kuala Lumpur, Malaysia.
[2]Department of Chemical Engineering, Ahmadu Bello University, 870001 Nigeria.
Email: ashri@um.edu.my, adeniyipee@live.com & ymsani@siswa.um.edu.my

Abstract. Crystalline solidacid catalysts exhibit higher catalytic activity and hydrothermal stability in catalytic cracking compared with their amorphous counterparts. This is because of the presence of stronger Brönsted acid sites on their surfaces. Thus, we report the synthesis of crystalline solidacid material by impregnating NaOH into the pores of thermal and acid-treated amorphous aluminosilicate. NH_3-TPD, XRD, TGA and DSC revealed the surface acidity, structural and textural properties of the materials. All the kaolinites peaks in the starting material disappeared after the thermal and acid activation. Interestingly, most of the crystalline peaks reappeared with greater intensities at the (0211) band after NaOH impregnation. Further, the crystallinity index calculated by weighted intensity ratio index (WIRI) at (0211) band showed superior crystallinity for the synthesized material than the starting kaolin. This is in consonant with reemerging crystalline peaks. The acidity … This work demonstrates that impregnation of NaOH on amorphous aluminosilicate is a novel route for synthesizing of crystalline superacid catalysts.

Keywords: *Solidacid catalyst; kaolinite; acid activation; alkali activation; crystallinity*.

1. Introduction

Biodiesel is renewable, sustainable and nonfossil based fuel with various advantages such as renewability, sustainability, biodegradability, lower GHG-emissions and enhanced lubricity [9]. Further, the prospect of producing biodiesel from existing refineries is promising. However, robust and active solidacid catalysts are essential for ensuring smooth transition into the refineries for commercial productions. Evidently, solidacid catalysts have gained wide acceptance in catalytic conversion processes such as bulk chemistry and petrochemical processes [1, 2]. However, cost of producing such catalysts remains major challenge hindering catalysis from ensuring the prominence of biodiesel. Hence, cheaper starting materials with equally high catalytic properties will help in alleviating the economic constraints. Interestingly, kaolinites clay minerals catalysts found industrial applications since the early 1930s. Significant progress in several industrial processes such as petrochemistry; especially catalytic refining and bulk chemistry became possible with kaolinite as precursor in active catalyst synthesis. This is because of the unique structure and pore size which are suitable for conversion of bulky molecules [3]. These explain the renewed interests that aluminosilicates from clay are receiving towards solidacid catalyst synthesis. However, kaolinites resist acid attack during activation because of higher octahedral alumina contents. Calcining at temperatures between 550 and 950 ˚C subdues this resistance by transforming the clay to metakaolin. Nonetheless, this transformation deforms the crystalline structure of the clay material.

A process for alleviating these issues is acid leaching of metakaolin. Development of porosity, acidity and surface area are the major significance of acid leaching. The process also dealuminates and purifies the octahedral layers to facilitate formation of surface structure. However, materials synthesized by this procedure are amorphous in nature. Therefore, there is a need to make the catalytic material crystalline for higher catalytic performances. This is

ISBN: 978-602-71398-0-0

because crystalline materials exhibit higher catalytic activity, high yields of gasoline, paraffinic and aromatic components because of their high hydrothermal stability. They also exhibit lower deactivation rates compared with synthetic amorphous aluminosilicates [10-12]. Initially, researchers synthesized solidacid catalysts for catalytic cracking for by lixiviation of kaolinites and bentonite clay [1]. Moreover, recent reports exhibited promising potentials of solidacid catalysts from clay for biodiesel production by esterification [4-6]. Similarly, [7] obtained encouraging results from transesterifying vegetable oil in excess methanol to produce biodiesel. The plausible reason to these is that solidacid catalysts catalyst enhance free fatty acids (FFA) conversion during biodiesel production [8]. Therefore, this study investigated the nature of Brönsted acid sites effect of and crystallization of thermal and acid treated amorphous aluminosilicates in synthesizing solidacid catalyst. The study also explored the effect of impregnating aqueous NaOH, crystallinity and physicochemical properties of the synthesized materials.

2. Experimental

2.1. Materials

Table 1 presents the physicochemical properties of the kaolin employed for this investigation as purchased from R&M Chemicals Sdn. Bhd., Malaysia. It is an ordered kaolinite with weighted intensity ratio index (WIRI) of 0.9151. The study utilized the reagents without further purification. R&M Chemicals Sdn. Bhd., Malaysia also supplied the NaOH and H_3PO_4 (85% pure).

2.2. Methods

2.2.1. Thermal and acid treatment of the kaolin

Calcination at 850 ˚C transformed the kaolin into metakaolin. This thermal process made the material more susceptible to dealumination and removal of impurities. 6M H_3PO_4 leached the metakaolin sample at 90 ˚C for 4 h. We divided the resulting solution into two parts after quenching with distilled water. A repetitive washing step on the first portion with distilled water achieved a pH value of 5. Conversely, mixing with predetermined amount of aqueous NaOH facilitated attaining same pH value of 5 on the second portion. We filtered both solutions separately with vacuum pump and dried them overnight at 120 ˚C. We designated the samples obtained from distilled water and NaOH solution pH adjustment as PLK8-6M4h and NaPLK8-6M4h respectively. The NaPLK8-6M4h samples were ion exchanged with 0.1 M NH_4NO_3 for 24 h. The resulting solution designated HPLK8-6M4h was filtered and dried overnight at 120 ˚C. The calcination condition for all synthesized materials is 550 ˚C for 2 h.

2.2.2. Characterization

The study employed X-ray diffraction analysis (XRD), XRF, FTIR, DSC and N_2 adsorption–desorption isotherms for characterizing the synthesized materials. PANanalytical X'pert Empyrean X-ray diffractometer with Cu*K*α radiation at 40 kV and 40 mA performed the XRD analysis. Similarly, Quantachrome Nova 1200 apparatus analyzed the N_2 adsorption–desorption isotherms at liquid nitrogen temperature. Outgassing at 130 ˚C for 2 h before each

ISBN: 978-602-71398-0-0

measurement ensured accurate results on all the samples. We employed t-plot methods and Brunauer–Emmett–Teller (BET) to analyze the specific surface area, microporous area, microporous volume and pore-size distribution, specific surface area respectively.

2.3. Crystallinity assessment

2.3.1. XRD method

Crystallinity is a function of the physical nature of the characteristic peaks. Broad peaks indicate low crystallinity while sharp X-ray peaks indicate high crystallinity. Therefore, to assess crystallinity index of the materials, we analyzed the XRD patterns. We employed the Aparicio-Galán-Ferrell (AGFI), Hinckley (HI) represented by Eq. 1 and 2; and weighted intensity ratio index (WIRI) with weighted intensity of (0 2 1 1) band in computing the indices.

$$AGFI = \frac{I_A + I_B}{2I_C} \quad (1)$$

However, HI (Eq. 2) is only applicable where the kaolinite content in the material is more than 20 wt%. For highly crystalline kaolinites, the HI value is greater than 1.0 while it is below 1.0 for kaolinites with low crystallinity [13]. Figure 1 illustrates the values of the individual peaks obtained from the XRD patterns.

$$HI = \frac{A+B}{A_h} \quad (2)$$

In contrast, WIRI (Eq. 3) defines crystallinity as function of peak intensities of (02, 11) band and full width half maximum (FWHM) of the corresponding 020, $1\bar{1}0$, $11\bar{1}$ and $1\bar{1}\bar{1}$ reflections resulting from decomposition of the same band [13, 14]. The weighting coefficients w_1, w_2, w_3 and w_4 in Eq. 3 are the reciprocal of FWHM of $1\bar{1}0$, $11\bar{1}$, $1\bar{1}\bar{1}$ and 020 peaks respectively[14]. The value of WIRI ranges between 0 and 1. It is $\leq$ 0.4, 0.4<WIRI$\leq$ 0.7 and 0.7 for low crystallinity, medium crystallinity and for high crystallinity respectively.

$$WIRI = 1 - e^{-\left(\frac{(w_1 I(1\bar{1}0) + w_2 I(11\bar{1}) + w_3 I(1\bar{1}\bar{1}))}{w_4 I(020)}\right)} \quad (3)$$

ISBN: 978-602-71398-0-0

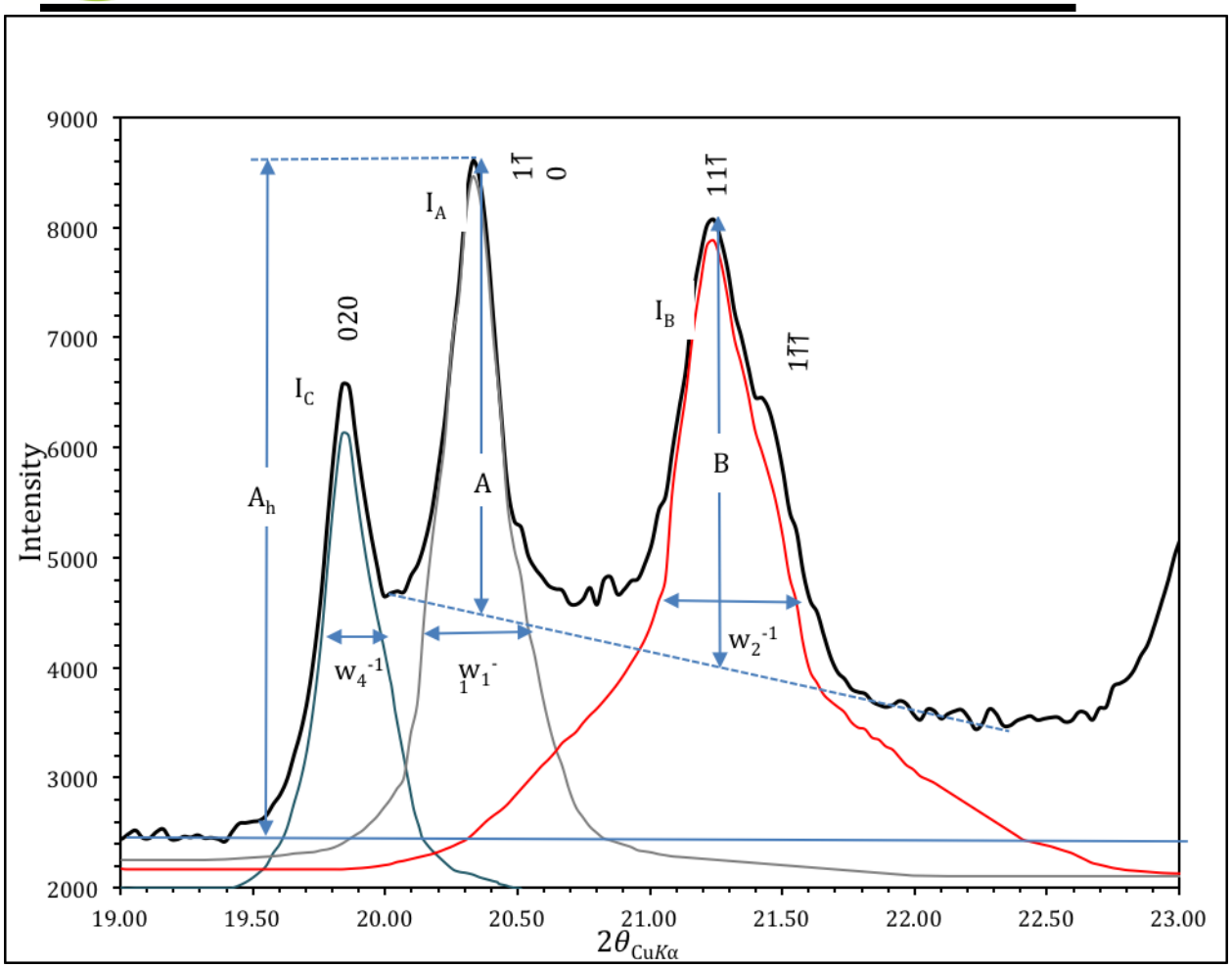

Figure 1 Computation of HI, AGFI and WIRI indices values from kaolin XRD data.

3. Results and discussion

3.1. Characterization

3.1.1. Chemical compositions

XRF data revealed the compositions of the kaolin and that of the synthesized materials from metakaolin. Table 1 presents a comparison between the compositional values obtained with that of theoretical kaolinite [15]. The characterization results revealed high TiO_2 content in the synthesized materials. Further, the acid-treated metakaolin showed reduced Al_2O_3 content (Si/Al ratio). We attributed these transformations to pH adjustment. A pH value of ~5 facilitates acid leaching of metakaolin and subsequent development of acid sites, porosity and surface area. Elucidate further from items on Table 1

[Insert Table 1 here]
Chemical compositions (wt%) of kaolin and treated metakaolinites.

ISBN: 978-602-71398-0-0

3.1.2. FTIR analysis

Figure 2 illustrates FTIR assignments of untreated kaolin and that of synthesized kaolinitic samples. Markedly, untreated kaolin spectrum exhibits unique bands at 3687, 3632 and 3620 cm^{-1} in the O-H stretching region (Figure 2a). This corresponds to the octahedral hydroxyl units ($Al\text{-}OH_{str}$) [16, 17]. The band at 3687 cm^{-1} displayed strong inner surface O-H in-phase stretching vibration. Similarly, the absorption band at 3620 cm^{-1} showed strong inner surface O-H stretching vibration between the tetrahedral and octahedral lamella of kaolin [16, 18]. Conversely, the inner surface OH out-phase stretching vibration found at 3632 cm^{-1} exhibited medium strength. Interestingly, these unique bands disappeared after calcining at 850 ˚C. We attributed this phenomenon to hydrogen bonds breakage between the layers of the kaolin because of thermal effect on the structural hydroxyl units. This paves way for a more severe acid leaching of the material. Equally, kaolin bending regions at 914, 789, 750, 684 and 530 cm^{-1} disappeared after calcination and acid leaching (Figure 2b). This leads to structural deformation of the material from crystalline to amorphous structure. This is consistent with the results revealed by XRD illustrated in (Figure 3). The disappearance is despite different vibrational directions of 914 and 530 cm^{-1} bands (Al-OH and Si-OH bending vibrations respectively) and 789, 750 and 684 cm^{-1} bands representing Al-OH ("gibbsite-like" layer) translational vibrations. These bands reappeared at the bending region (Figure 2b) as exhibited by synthesized NaPLK8-6M4h samples. We ascribed this transformation to crystalline structure restoration in the catalytic material. However, because of increase in Si/Al ratio, the peak intensities of NaPLK8-6M4h samples were lower than that of the untreated kaolin.

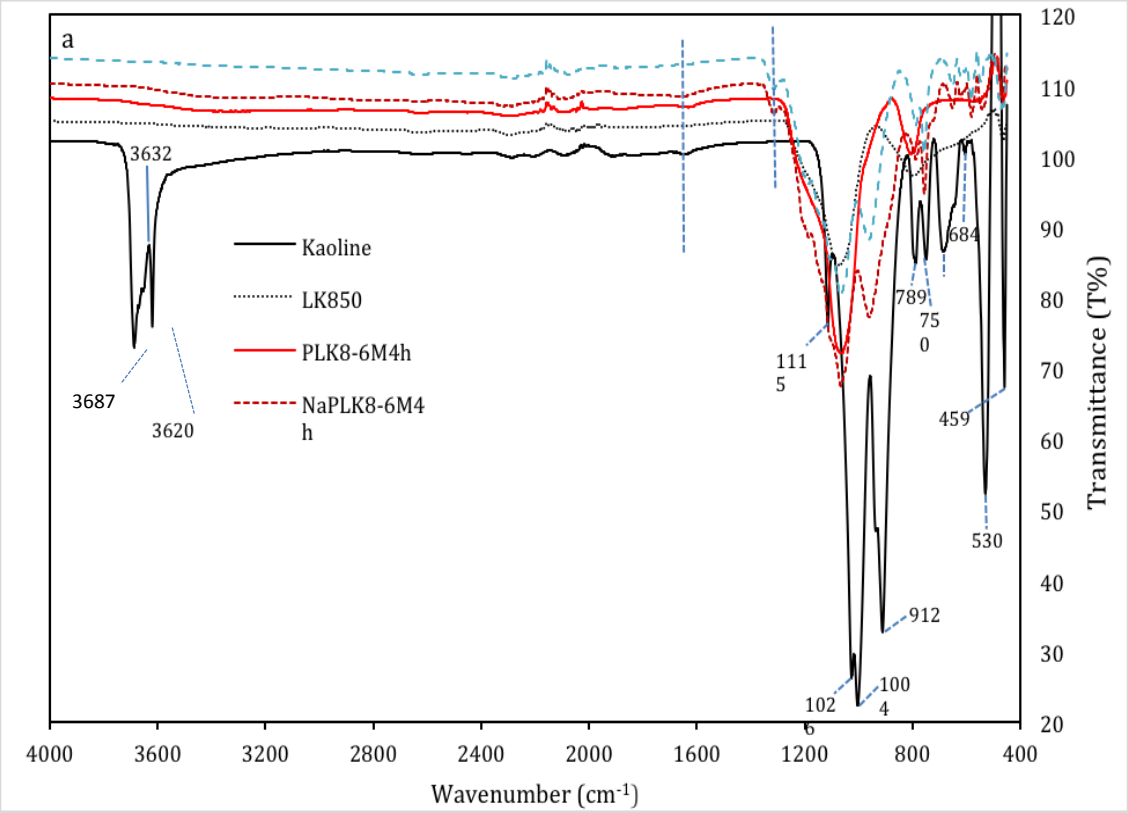

ISBN: 978-602-71398-0-0

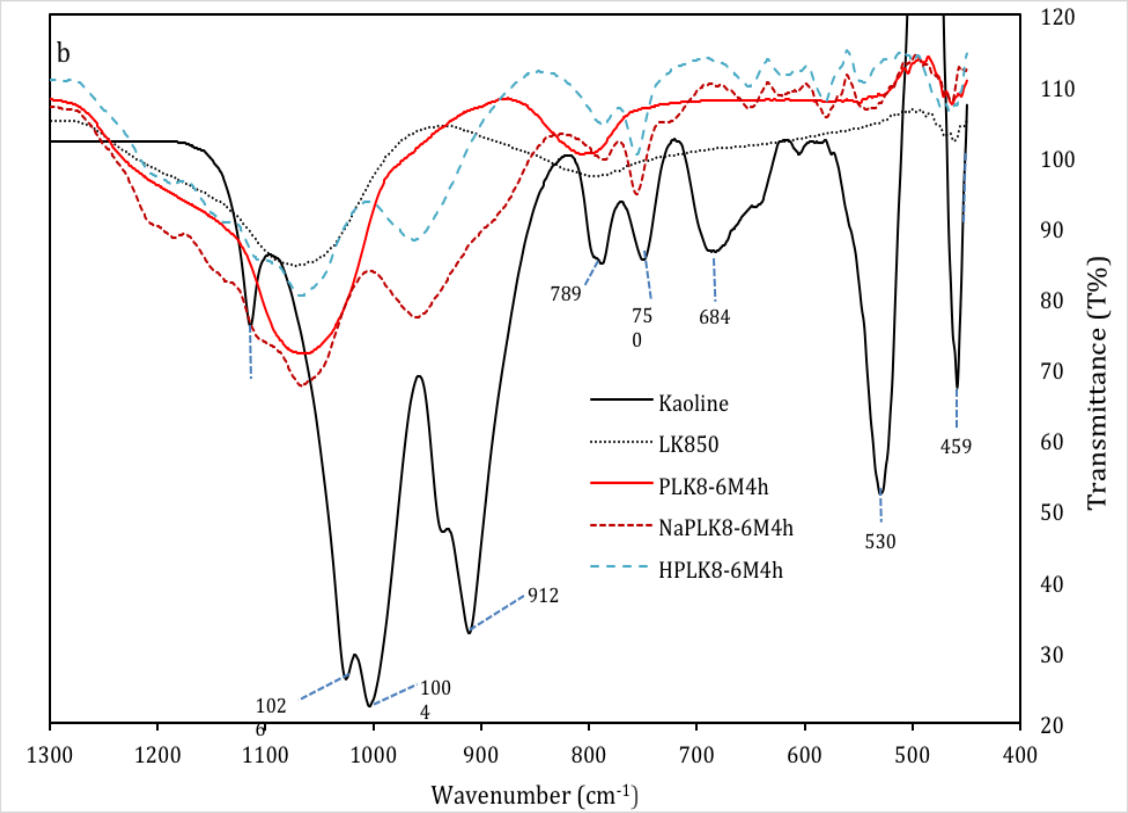

Figure 2 FTIR spectra of untreated kaolin and synthesized kaolinites.

3.1.3. N_2 adsorption–desorption

3.1.4. X-ray diffractograms analysis

Several studies [ref] have shown the possibility of detecting major variances such as crystallinity index for different kaolinitic materials within the range of $20°<2\theta>24°$. Transformation of kaolin to metakaolin at 850°C for 2 h leads to water loss and disappearance of all the kaolinite peaks. However, attaching anatase (TiO_2) and quartz replaces the peaks with a broadband peak in the range of $20°<2\theta>30°$. This is associated with the presence of amorphous SiO_2 [3] and increase in anatase composition. This is represented by the appearance of three peaks at 26.61°, 48°and 55° [Figure]. Conversely, the disappearance of the peak at 001 basal plane (2θ) is traceable to hydrogen bonds breakage between the layers of kaolinite. This structural water loss transformed the octahedral alumina unit into penta- and tetrahedral coordinated alumina unit [2, 19]. Further, it exposed the material to acid attack by partial dissolution of Al^{3+}. Consequently, the acid treated metakaolin (PLK8-6M4h) exhibited similar XRD pattern to that of the metakaolin but with increased amorphous phase. Nonetheless, XRD pattern for the commercial kaolin showed characteristic peaks at 2θ values of 12.34° and 24.87° (Figure 3I). The XRD pattern of NaOH-adjusted material (NaPLK8-6M4h) displayed reemergence of the peak at 001 basal plane (2θ) but with a very low intensity. We ascribed this to bonding of hydrogen bonds between the layers of the materials. Interestingly, the process of ion exchange increased the intensity of all the peaks as exhibited by samples designated HPLK8-6M4h. Further, intensity of peaks in the range of $20°<2\theta>24°$ got restored.

3.2. Crystallinity assessment

ISBN: 978-602-71398-0-0

Figure 3II illustrates the variances in the X-ray diffractograms of untreated commercial kaolinite and synthesized materials. The complete disappearance of kaolinite peaks was evident from PLk8-6M4h diffractograms except for the peak in the range of $20°<2\theta>24°$. Therefore, to determine crystallinity indices, we analyzed the diffraction (02, 11) intensities in this range. Table 3 presents the results of the crystallinity indices as computed according to Equations (1) to (3).

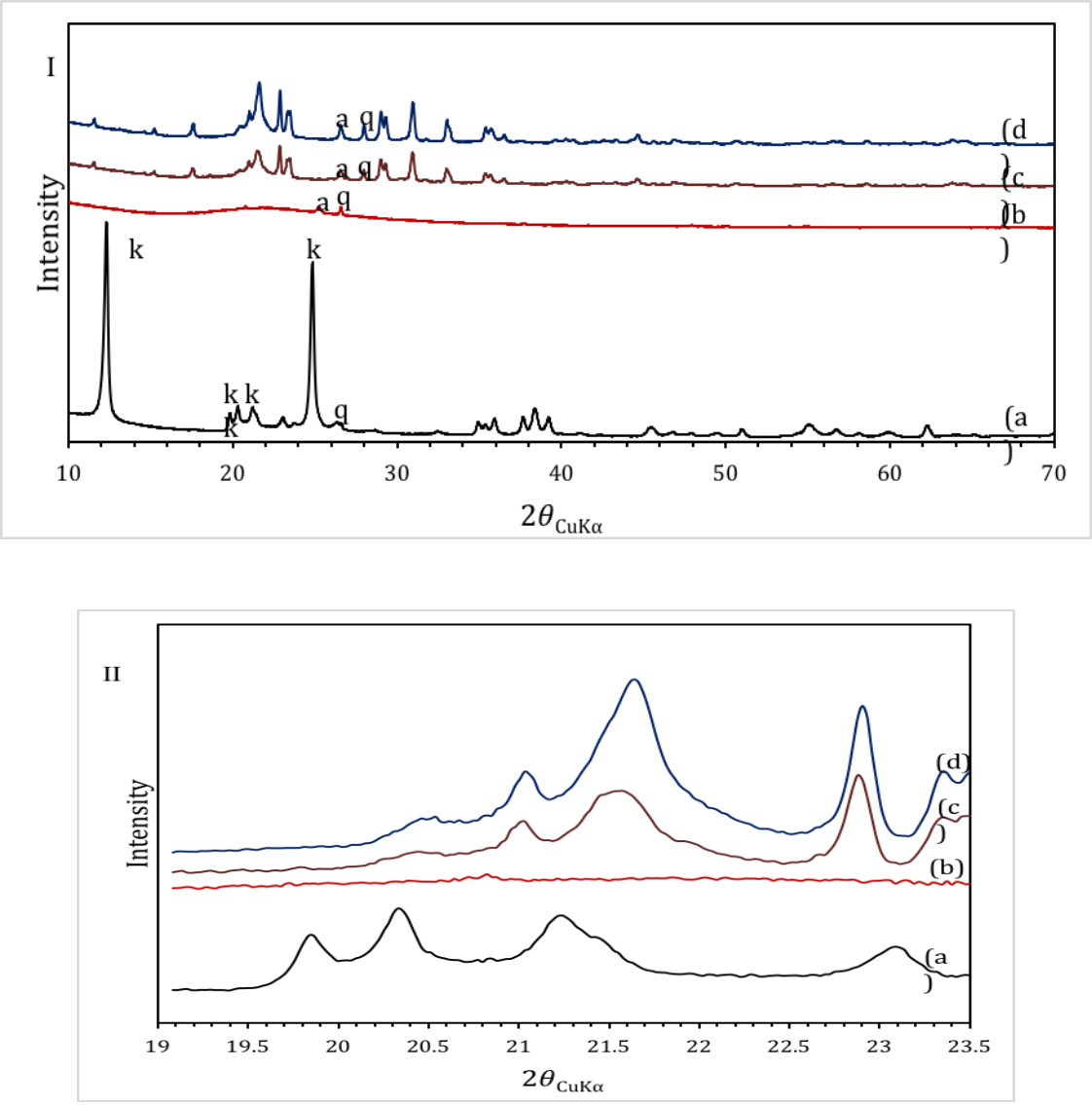

Figure 3 XRD pattern for kaolinite (a), PLk8-6M4h (b), NaPLk8-6M4h (c) and HPLk8-6M4h (d).

Table 2 Density and crystallinity indices of the kaolinite materials

ISBN: 978-602-71398-0-0

Samples	ρ (g/c m^3)	Indices		
		HI	AGFI	WIRI
Kaolinite	0.4934	1.328	1.429	0.9151
LK8	0.4739	-	-	-
PLk8-6M4h	0.3373	-	-	-
NaPLk8-6M4h	0.6669	2.000	2.845	0.9999
HPLK8-6M4h	0.6657	2.490	3.892	0.9997

"Among advantages of application of the WIRI belong: (1) Values of WIRI oscillate between 0 and 1 (as usual for index). (2) Weighting intensities are better for resolution of degree of disorder in kaolin samples than only non-weighting ones. (3) Utilization of decomposition procedure to obtain ''pure'' intensity profiles of overlapped reflections [13]".

This observation corroborates the report of Sato et al. [20] that ion exchange reduces crystallinity of sodium aluminosilicates. However, the reduction in crystallinity was minimal at high Si/Al ratio from this study.

Reference

[1] Perissinotto, M., et al., *Solidacid catalysts from clays: Acid leached metakaolin as isopropanol dehydration and 1-butene isomerization catalyst.* Journal of Molecular Catalysis A: Chemical, 1997. **121**(1): p. 103-109.

[2] do Nascimento, L.A.S., et al., *Comparative study between catalysts for esterification prepared from kaolins.* Applied Clay Science, 2011. **51**(3): p. 267-273.

[3] Lenarda, M., et al., *Solidacid catalysts from clays: preparation of mesoporous catalysts by chemical activation of metakaolin under acid conditions.* Journal of colloid and interface science, 2007. **311**(2): p. 537-543.

[4] da Silva Lacerda Junior, O., et al., *Esterification of oleic acid using 12-tungstophosphoric supported in< i> flint</i> kaolin of the Amazonia.* Fuel, 2013.

[5] de Oliveira, A.d.N., et al., *Microwave-assisted preparation of a new esterification catalyst from wasted< i> flint</i> kaolin.* Fuel, 2012.

[6] Patel, A. and V. Brahmkhatri, *Kinetic study of oleic acid esterification over 12-tungstophosphoric acid catalyst anchored to different mesoporous silica supports.* Fuel Processing Technology, 2013. **113**: p. 141-149.

[7] Dang, T.H., B.-H. Chen, and D.-J. Lee, *Application of kaolin-based catalysts in biodiesel production via transesterification of vegetable oils in excess methanol.* Bioresource technology, 2013. **145**: p. 175-181.

ISBN: 978-602-71398-0-0

[8] Boz, N., N. Degirmenbasi, and D.M. Kalyon, *Conversion of biomass to fuel: Transesterification of vegetable oil to biodiesel using KF loaded nano-γ-Al< sub> 2</sub> O< sub> 3</sub> as catalyst.* Applied Catalysis B: Environmental, 2009. **89**(3): p. 590-596.

[9] do Nascimento, L.A.S., et al., *Esterification of oleic acid over solidacid catalysts prepared from Amazon< i> flint</i> kaolin.* Applied Catalysis B: Environmental, 2011. **101**(3): p. 495-503.

[10] Tan, Q., et al., *Synthesis, characterization, and catalytic properties of hydrothermally stable macro–meso–micro-porous composite materials synthesized via in situ assembly of preformed zeolite Y nanoclusters on kaolin.* Journal of Catalysis, 2007. **251**(1): p. 69-79.

[11] Mohammed, A., S. Karim, and A.M. Rahman, *Characterization and Cracking Activity of Zeolite Prepared from Local Kaolin.* Iraqi Journal of Chemical and Petroleum Engineering, 2010. **11**: p. 35-42.

[12] Corma, A., et al., *Cracking activity and hydrothermal stability of MCM-41 and its comparison with amorphous silica-alumina and a USY zeolite.* Journal of catalysis, 1996. **159**(2): p. 375-382.

[13] Chmielová, M. and Z. Weiss, *Determination of structural disorder degree using an XRD profile fitting procedure. Application to Czech kaolins.* Applied clay science, 2002. **22**(1): p. 65-74.

[14] Ptáček, P., et al., *The influence of structure order on the kinetics of dehydroxylation of kaolinite.* Journal of the European Ceramic Society, 2013.

[15] Carneiro, B., et al., *Mineralogical and geochemical characterization of the hard kaolin from the Capim region, Pará, northern Brazil.* Cerâmica, 2003. **49**(312): p. 237-244.

[16] Ayodele, O.B., *Effect of phosphoric acid treatment on kaolinite supported ferrioxalate catalyst for the degradation of amoxicillin in batch photo-Fenton process.* Applied Clay Science, 2013.

[17] Hu, P. and H. Yang, *Insight into the physicochemical aspects of kaolins with different morphologies.* Applied Clay Science, 2012.

[18] Panda, A.K., et al., *Effect of sulphuric acid treatment on the physico-chemical characteristics of kaolin clay.* Colloids and Surfaces A: Physicochemical and Engineering Aspects, 2010. **363**(1): p. 98-104.

[19] Massiot, D., et al., *27Al and 29Si MAS NMR study of kaolinite thermal decomposition by controlled rate thermal analysis.* Journal of the American Ceramic Society, 1995. **78**(11): p. 2940-2944.

ISBN: 978-602-71398-0-0

[20] Sato, K., et al., *Structural changes of Y zeolites during ion exchange treatment: effects of Si/Al ratio of the starting NaY.* Microporous and mesoporous materials, 2003. **59**(2): p. 133-146.